Chemical-potential flow equations for graphene with Coulomb interactions

Christian Fräßdorf[1] and Johannes E. M. Mosig[2]
[1]*Dahlem Center for Complex Quantum Systems and, Institut für Theoretische Physik, Freie Universität Berlin, Arnimallee 14, 14195 Berlin, Germany*
[2]*Department of Mathematics and Statistics, University of Otago, PO Box 56, Dunedin 9054, New Zealand*

(Received 13 July 2017; revised manuscript received 22 March 2018; published 11 June 2018)

We calculate the chemical potential dependence of the renormalized Fermi velocity and static dielectric function for Dirac quasiparticles in graphene nonperturbatively at finite temperature. By reinterpreting the chemical potential as a flow parameter in the spirit of the functional renormalization group (fRG) we obtain a set of flow equations, which describe the change of these functions upon varying the chemical potential. In contrast to the fRG the initial condition of the flow is nontrivial and has to be calculated separately. Our results are consistent with a charge carrier-independent Fermi velocity $v(k)$ for small densities $n \lesssim k^2/\pi$, supporting the comparison of the zero-density fRG calculation of Bauer *et al.* [Phys. Rev. B **92**, 121409 (2015)], with the experiment of Elias *et al.* [Nat. Phys. **7**, 701 (2011)].

DOI: 10.1103/PhysRevB.97.235415

I. INTRODUCTION

The spectrum of free electrons in graphene is characterized by two Dirac points around which the energy disperses linearly as a function of momentum [1–3]. One important peculiarity of the linear band structure is that it leads to a vanishing density of states at these nodal points. The vanishing charge carrier density implies the absence of screening, leading to strongly enhanced corrections of the system's single-particle properties by the long-range tail of the Coulomb interaction. One-loop calculations have shown that the Fermi velocity acquires logarithmic corrections upon approaching the nodal points [4–7]. These corrections diverge precisely at the nodal points at zero temperature, which corresponds to a strongly increasing Fermi velocity.

This effect becomes most pronounced in the strong coupling regime, which is experimentally realized by freestanding graphene, where there is no screening dielectric surrounding the graphene sheet. Such an experiment has been performed recently by Elias *et al.* [8], with the goal to experimentally verify the predicted logarithmic divergence of the velocity near the nodal points. Since perturbative calculations are not reliable in such a situation—the dimensionless interaction strength in freestanding graphene is about 2.2—nonperturbative methods have been employed for a quantitative theory of this effect. Bauer *et al.* [9] used the functional renormalization group (fRG) formalism to access the strong coupling regime [10–13], finding excellent agreement with the experiment of Elias *et al.* Upon closer inspection, however, the calculation of Ref. [9] addresses a slightly different quantity than what is measured in the experiment of Ref. [8]. The theoretical calculation has been performed at zero density and equates the momentum dependent quasiparticle velocity $v(k)$ with the Fermi velocity in a system with finite carrier density at Fermi momentum $k = k_F$. The experiment, in contrast, observed the logarithmic increase of the Fermi velocity as a function of the charge carrier density $n = k_F^2/\pi$. Strictly speaking these two velocities are different aspects of a more general velocity function, $v(k,\mu,T)$, which depends on momentum k, chemical potential μ (or the carrier density n, respectively), and temperature T. Equating the velocities of Refs. [8] and [9] requires that the carrier density dependence of the full velocity function is negligible for $n \lesssim k^2/\pi$. This identification allows one to map the momentum dependence to a density dependence, which could then be compared to the experiment. It is the goal of this paper to provide a theoretical framework for a nonperturbative calculation of the velocity function $v(k,\mu,T)$ and to calculate the density dependence of the static dielectric function.

Within a standard application of the fRG to calculate the renormalization of the Fermi velocity at finite density one faces the challenge that a renormalization of the Fermi surface under the RG flow has to be accounted for. The feature of a flowing Fermi surface is typically accompanied by significant technical complications regarding its implementation in certain cutoff and truncation schemes used in the literature [12,13]. Furthermore, studying an actual functional chemical potential dependence of correlation functions is numerically very expensive, since it requires a repeated solution of the truncated vertex flow equations for every value of the chemical potential. To circumvent both complications, we here explore a variant of the fRG, where the chemical potential μ is interpreted as a flow parameter [14,15], in combination with nontrivial input from a prior nonperturbative calculation at charge neutrality [9,16]. In contrast to conventional fRG where one is only interested in the one-particle irreducible vertex functions at the end of the flow, the chemical-potential flow bears physical information for all values of the flow parameter. The solution to the chemical-potential flow equations directly gives access to the full μ dependence of the vertex functions. Of particular importance in the chemical-potential flow is the initial condition. Among others it contains the information about the renormalization of the spectrum—and hence the interacting Fermi surface—at the initial chemical potential μ_0 (the latter being zero

at the charge neutrality point). A further renormalization of the spectrum and Fermi surface at different values for the chemical potential, $\mu \neq \mu_0$, is then taken care of by the flow itself.

In the ideal case—that is if the fRG equations could be solved exactly—the chemical-potential flow and the conventional fRG, where the flow equations are solved for each μ separately, yield the same answer. However, since there are always approximations involved by truncating the flow equations at a finite order, the solutions one obtains in the two approaches need not be equal. Hence the chemical-potential flow should be regarded as a complementary approach to the conventional finite density fRG to study density dependences. Since the chemical-potential flow has attracted much less attention in comparison to its standard fRG counterpart, there are no extensive studies whether the typical low-level truncation schemes, that are employed in the standard finite density fRG framework, are sufficient for a chemical potential-based flow, and to what extent their respective outcomes are quantitatively comparable. Due to the lack of finite-density fRG calculations for graphene, which could serve as a benchmark for the method we want to employ here, we may resort to the existing perturbative calculations for the self-energy and polarization function, which—among others—have been carried out in Refs. [17] and [18], respectively. Although such calculations should be a good approximation in the weak coupling regime only, but certainly not for strong coupling we study here, their predictions at least yield a qualitative reference point for a comparison. Nevertheless, graphene is an ideal testing ground for our method, due to the available experimental data for the strong coupling regime.

In the present paper we use a minimal truncation that only takes into account the flow of the renormalized Fermi velocity and dielectric function. As we will explain in the main part of this work, this represents a rather crude approximation. While the resulting μ-dependent dielectric function appears to be consistent with the expectations from one-loop perturbation theory, the results for the renormalized Fermi velocity are not satisfactory for large densities $n \gtrsim k^2/\pi$. For the low and intermediate density regime, $n \lesssim k^2/\pi$, we find a negligible density dependence of $v(k,\mu,T)$, consistent with the approximations made in Ref. [9]. In spite of the deficiencies of the simple truncation scheme studied here, the chemical-potential flow method is open to systematic improvements through higher order truncations, which we leave for future work.

The outline of the paper is as follows. In Sec. II we introduce the microscopic continuum model of interacting graphene electrons, we briefly discuss the general idea behind the chemical-potential flow and its difference to the standard fRG, followed by the truncation that is employed in this paper. In Sec. III we present the numerical solution and discuss the results. We conclude in the final section. Details about the derivation of the chemical-potential flow equation for the effective action, the vertex flow equations for the one-particle irreducible vertex functions, and their corresponding one-loop approximations are shown in two appendixes. The one-loop flow equations allow for a direct derivation of the results obtained in Refs. [17] and [18] within the chemical-potential flow framework.

II. MODEL AND FLOW EQUATIONS

Interacting Dirac fermions in graphene are described by the Hamiltonian ($\hbar = 1$) [19]

$$H_\mu = -\int_{\vec{r}} \Psi^\dagger(\vec{r})\big(\mu + i v_F \sigma_0^s \otimes \vec{\Sigma}\cdot\vec{\nabla}\big)\Psi(\vec{r}) + \frac{1}{2}\int_{\vec{r},\vec{r}'} \delta n_\mu(\vec{r}) \frac{e^2}{\epsilon_0|\vec{r}-\vec{r}'|}\delta n_\mu(\vec{r}'), \tag{1}$$

with $\delta n_\mu(\vec{r}) = \Psi^\dagger(\vec{r})\Psi(\vec{r}) - \tilde{n}_\mu(\vec{r})$. The Dirac electrons are described by eight-component spinors $\Psi \equiv (\Psi_\uparrow \quad \Psi_\downarrow)^\intercal$, with $\Psi_\sigma \equiv (\psi_{AK_+}\ \psi_{BK_+}\ \psi_{BK_-}\ \psi_{AK_-})^\intercal_\sigma$. The indices $\sigma = \uparrow, \downarrow$ denote the spin, $K_\pm$ the valley, and A/B the sublattice degree of freedom. Furthermore, σ_0^s is the two-dimensional unit matrix acting in spin space and $\Sigma_{1,2} = \tau_3 \otimes \sigma_{1,2}$ are four-dimensional matrices, with the Pauli matrices τ_3 and $\sigma_{1,2}$ acting in valley and sublattice space, respectively. The term $\tilde{n}_\mu(\vec{r})$ is a background charge density, which depends implicitly on the chemical potential. It represents the charge accumulated on a nearby metal gate and removes the zero wave number singularity of the bare Coulomb interaction. Furthermore, the constant ϵ_0 in the denominator of the Coulomb interaction amplitude is the dielectric constant of the medium, which accounts for the screening effects of a substrate or a surrounding dielectric on the bare Coulomb interaction. For freestanding graphene it is equal to one.

The key insight of our method is that the chemical potential in Eq. (1) couples to a fermion bilinear in exactly the same way as an additive infrared regulator in the fRG. Since the Hamiltonian is a continuous and differentiable function of μ, the chemical potential may formally be reinterpreted as a flow parameter [14,15]. This interpretation enables us to derive an exact flow equation for the chemical potential-dependent effective action Γ_μ and to apply the by now well-established methods of the fRG. Since the essential steps to arrive at an exact flow equation are identical to the fRG, we can immediately transfer the general (finite temperature and density) fRG equations from Ref. [16], taking care that the regularization prescription is substituted appropriately. In Fig. 1 we show a graphical representation of the truncated flow equations for the one-particle irreducible vertex functions of the theory in its Fermi-Bose form. The bosonic field was introduced by a Hubbard-Stratonovich transformation of the Coulomb interaction in the density-density channel [9,13,16,20–22].

In contrast to the standard fRG the main issue of concern in the chemical-potential flow theory is the initial condition of the flow. Since the chemical potential is different from an infrared regulator by its analytical structures, the effective action at some—arbitrarily chosen—initial chemical potential μ_0 is nontrivial in general. In particular, it typically does not coincide with the bare action, but already contains the full information about thermal and quantum fluctuations. Formally, the exact initial condition Γ_{μ_0} requires the knowledge of an infinite set of vertex functions, which—for obvious reasons—is impossible to obtain, but instead has to be approximated reasonably well by a separate calculation, using an appropriate nonperturbative method such as the fRG or Schwinger-Dyson equations [23], for example [24]. Such a preceding calculation is essential for the chemical-potential flow as the differential

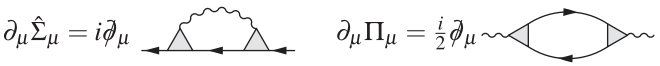

FIG. 1. Graphical representation of the chemical potential flow equations for the self-energy $\hat{\mathbf{\Sigma}}_\mu$ and the polarization function $\mathbf{\Pi}_\mu$. Contributions from higher order vertices $\mathbf{\Gamma}_\mu^{(m,n)}$, with $m > 2, n > 1$ are already neglected. Straight and wiggly lines represent the flowing fermionic and bosonic propagators, respectively, and the shaded triangle represents the Fermi-Bose three-vertex $\mathbf{\Gamma}_\mu^{(2,1)}$. The derivative $\partial\!\!\!/_\mu$ on the right hand side only acts on the flowing fermionic propagators, substituting the latter by the so-called single scale propagator [16]. An analytical representation of these flow equations is given in Appendix B.

flow equations gain quantitative predictive power through the correct initial condition only. Apart from the truncation of the chemical-potential flow equations, the necessity to truncate the infinite dimensional theory space of the initial effective action to a finite dimensional subspace represents another level of approximation that is absent in the standard fRG and has to be dealt with with care.

One such issue we want to discuss briefly are Ward identities. In the standard fRG formalism Ward identities are modified due to the introduction of an artificial infrared regulator. Only at the end of the flow—that is at $\Lambda = 0$, where the infrared cutoff is removed—the modified Ward identities assume their original form. In a particular truncation of the standard fRG equations one has to make sure that those modified Ward identities are fulfilled at each value of the flowing cutoff, in particular at the end of the flow. Within the chemical-potential flow formalism, on the other hand, the Ward identities themselves are not modified at all, because the bare action requires no modification. Since the calculation of the initial condition relies on certain approximations, one has to make sure that those approximations are compatible with the Ward identities. Otherwise the initial condition would introduce an error that would simply be propagated by the chemical-potential flow, leading to results that are not reliable.

To calculate the initial condition for the present work we have chosen to use the Keldysh-fRG framework [25–32] we implemented in Ref. [16]. In that work, we calculated the Fermi velocity and the static dielectric function as functions of momentum and temperature at zero carrier density, finding full agreement with the previously established zero temperature results of Ref. [9]. The charge neutrality point was chosen, because it allows for a rather simplistic truncation, which is based on the dominance of a single interaction channel: the density-density channel, pronouncing forward scattering. Furthermore, technical complications arising from a renormalization group flow of the Fermi surface are avoided, since at $\mu_0 = 0$ the Fermi surface collapses to a point that is invariant under renormalization [33]. The truncation scheme in Refs. [9] and [16] neglects any dynamical effects, such as plasmons and the quasiparticle wave function renormalization, the three-vertex renormalization, and higher-order vertices entirely. We note that this truncation is compatible with an approximate Ward identity, which connects the marginal three-vertex renormalization with the quasiparticle wave function renormalization as shown in Ref. [9]. We use these results as the starting point of the chemical-potential flow.

Drawing inspiration from the initial fRG calculation, we employ the same level of truncation and the same approximations for the chemical potential-based flow. (For a more elaborate discussion regarding the justification of this truncation, see the end of this section.) That means, in particular, we limit ourselves to the flow of the isotropic quasiparticle pole (temperature arguments are suppressed throughout, if not stated otherwise),

$$\xi_\mu(k) \equiv v_\mu(k)k, \tag{2}$$

and the flow of the static dielectric function,

$$\epsilon_\mu(\vec{q}) \equiv \epsilon_0\big(1 + V(\vec{q})\Pi_\mu^{R/A}(\omega = 0, \vec{q})\big). \tag{3}$$

Here, we put the functional μ dependence as an index to resemble standard fRG notation. The renormalized and μ-dependent Fermi velocity $v_\mu(k)$ has been defined as $v_\mu(k) = v_F + \Sigma_{v,\mu}(k)$ [9,16] and $V(\vec{q}) = 2\pi e^2/\epsilon_0 q$ is the Fourier transform of the bare Coulomb interaction. Assuming the absence of spontaneous chiral symmetry breaking, we obtain two coupled flow equations from the general vertex flow equations shown in Fig. 1: one for the Fermi velocity $v_\mu(k)$ and one for the static dielectric function $\epsilon_\mu(q)$; see Appendix B for details. For convenience we introduce the function $\chi_\mu(q) \equiv \epsilon_\mu(q)q$, which is—up to constants—the algebraic inverse of the renormalized Coulomb interaction, and we state the two flow equations in terms of $\xi_\mu(k)$ and $\chi_\mu(q)$ ($k_B = 1$),

$$\partial_\mu \xi_\mu(k) = \frac{e^2}{4\pi}\int_0^\infty dq \int_0^\pi d\varphi\, \frac{1}{2T}\left(\cosh^{-2}\left(\frac{\xi_\mu(q)+\mu}{2T}\right) - \cosh^{-2}\left(\frac{\xi_\mu(q)-\mu}{2T}\right)\right)\frac{q\cos\varphi}{\chi_\mu(\sqrt{q^2+k^2-2qk\cos\varphi})}, \tag{4}$$

$$\partial_\mu \chi_\mu(q) = -\frac{e^2 q^2}{4\pi T}\int_0^\infty d\rho \int_0^\pi d\phi \left[\sum_{\nu=\pm1}\nu\left(\cosh^{-2}\left(\frac{\xi_\mu(\mathcal{Q}_-)-\nu\mu}{2T}\right) + \cosh^{-2}\left(\frac{\xi_\mu(\mathcal{Q}_+)-\nu\mu}{2T}\right)\right)\frac{\sin^2\phi}{\xi_\mu(\mathcal{Q}_-)+\xi_\mu(\mathcal{Q}_+)}\right.$$
$$\left. + \sum_{\nu=\pm1}\nu\left(\cosh^{-2}\left(\frac{\xi_\mu(\mathcal{Q}_-)-\nu\mu}{2T}\right) - \cosh^{-2}\left(\frac{\xi_\mu(\mathcal{Q}_+)-\nu\mu}{2T}\right)\right)\frac{\sinh^2\rho}{\xi_\mu(\mathcal{Q}_-)-\xi_\mu(\mathcal{Q}_+)}\right]. \tag{5}$$

These equations are supplemented by the nonperturbative initial conditions [16]

$$\xi^{\mathrm{fRG}}_{\mu_0=0}(k) = v^{\mathrm{fRG}}_{\mu_0=0}(k)k, \quad \chi^{\mathrm{fRG}}_{\mu_0=0}(q) = \epsilon^{\mathrm{fRG}}_{\mu_0=0}(q)q. \tag{6}$$

We emphasize once more that they are essential to obtain quantitatively reliable results. For example, the function $v^{\mathrm{fRG}}_{\mu_0=0}(k)$ contains logarithmic momentum corrections to the bare Fermi velocity v_F at charge neutrality, that cannot be generated by the

above flow equations. Naively using the bare Fermi velocity as initial condition would yield meaningless results.

In Eq. (5) the quantity $\mathcal{Q}_\pm$ is a short hand notation for the function $\mathcal{Q}_\pm(\rho,\phi,q) = \frac{1}{2}q\,(\cosh\rho \pm \cos\phi)$, where ρ and ϕ are elliptic coordinates, and the summation over $\nu = \pm 1$ covers the valence and conduction band. The derivation of the flow equations makes use of the particle-hole and chiral symmetries of the low energy Dirac model. As a result, the flow equations are fully symmetric with respect to the sign of μ, and the spectrum remains gapless and isotropic, leading to a circularly shaped Fermi surface defined by the equation $\xi_\mu(k_F)\pm\mu=0$ [34]. Deviations from isotropy, most importantly trigonal warping, are expected to occur only for very large values of μ, which are of the order of the upper band cutoff Λ_0 of the Hamiltonian (1). For a systematic study of those nonisotropic corrections one would need to modify the quadratic part of the Hamiltonian (1) by including terms that are of second order in the spatial derivatives, which derive from a second order $k\cdot p$ approximation [3]. Within the minimal truncation employed here such contributions would modify the flow equation of the dielectric function and, additionally, lead to a more complex flow equation for the then nonisotropic quasiparticle pole or, alternatively, another flow equation, associated to the deviation from isotropy. In addition, it would be necessary to calculate the proper initial condition for such a deviation by nonperturbative means. The hyperbolic cosines appearing in the flow equations are a consequence of the single-scale derivative ∂_μ acting on the fermionic distribution functions, the latter being part of the fermionic Keldysh propagator; see Appendixes A and B. In the limit of vanishing temperature the inverse hyperbolic cosine is proportional to a delta function, centered at the interacting Fermi surface. For finite, not too large temperatures the delta-function singularity is smeared out, but remains strongly peaked at the Fermi surface $\xi_\mu(k_F) \pm \mu = 0$, whereas those modes for which $\xi_\mu(k) \pm \mu \gg 2T$ are exponentially suppressed. Hence the momentum integrals of the two flow equations are finite, both in the ultraviolet and infrared regime [14]. Due to the particle-hole symmetry we may restrict the analysis to positive μ, i.e., n doping.

Before discussing the numerical solution of the flow equations we want to elaborate on the level of truncation. While the single channel truncation of the conventional fRG calculation at charge neutrality is justified by the dominance of the density-density channel, no such simplification can be made at finite density. It is expected that with increasing carrier density the other interaction channels gain in significance leading to the significantly more complex scenario of multiple competing interaction channels, see, e.g., Refs. [12,13,15], even before nonisotropic corrections become relevant [35]. The information about those additional interaction channels is encoded in the higher order vertices (most importantly the three- and four-vertices), whose contribution to the flow has already been neglected. We remind the reader that the above truncation is minimal in the sense that it only takes into account the flow of those quantities, which have been obtained by the initial fRG calculation. To be clear, there is no rigorous justification for such a low level truncation, such that a critical reflection of our results is necessary. Yet, it was deliberately chosen, since it allows for a clear identification of the effects of this single interaction channel, which makes it easy to understand the conceptual similarities and differences to the conventional fRG approach. Furthermore, as we show in Appendix B, after certain approximations are made our flow equations for the self-energy and the polarization function can be reduced to a differential form of the corresponding equations that are found within diagrammatic one-loop perturbation theory, the latter of which have been calculated in Refs. [17,18] for the fermionic self-energy and bosonic polarization in graphene, respectively. Hence the solution of the flow equations (4) and (5) represents a direct generalization of those perturbative results, which incorporates the mutual effects of Fermi velocity renormalization and charge carrier induced screening in a selfconsistent manner.

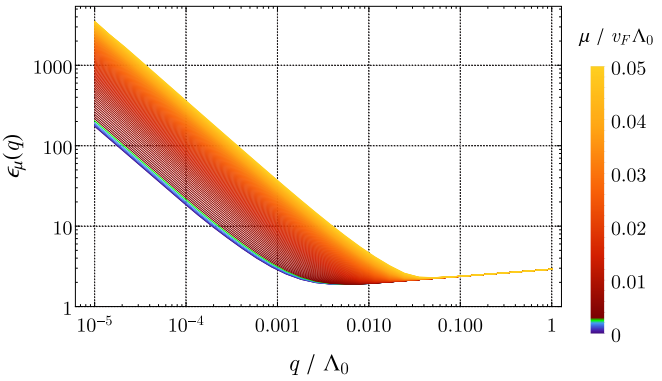

FIG. 2. Dielectric function $\epsilon_\mu(q)$ as a function of momentum and chemical potential at the reduced temperature $T/v_F\Lambda_0 = 2.5\times10^{-3}$. The colors blue to green and red to orange separate the two regimes $\mu \leqslant T$ and $\mu > T$, respectively. At the charge neutrality point the long range tail of the bare Coulomb interaction is cut off, due to thermal screening.

III. NUMERICAL RESULTS AND DISCUSSION

The flow equations (4) and (5) together with their initial conditions, Eq. (6), have been solved numerically for different temperatures with the dimensionless coupling constant $\alpha = e^2/\epsilon_0 v_F = 2.2$ appropriate for freestanding graphene [3,7,9].

The numerical results for the dielectric function are shown in Fig. 2 for the reduced temperature $T/v_F\Lambda_0 = 2.5\times10^{-3}$. Recall that Λ_0 is the upper band cutoff of the low-energy Hamiltonian (1). At the charge neutrality point the dielectric function shows a distinctively different behavior in the two momentum regimes $q > T/v_F$ and $q < T/v_F$. While the dielectric function is only weakly dependent on the momentum in the regime $q \gg T/v_F$, a strong $1/q$ divergence can be observed for $q \ll T/v_F$. As explained in Ref. [16], this divergence could be attributed to thermally induced charge carriers. In the presence of a finite chemical potential, that is excess charge carriers, the large momentum components of the dielectric function remain unaffected, whereas the initial $1/q$ divergence found in the low momentum regime becomes strongly enhanced, leading to an increasingly short ranged renormalized Coulomb interaction. This picture is consistent with the results obtained in one-loop perturbation theory. For comparison, in the regime $q \ll T/v_F$ perturbation theory predicts a polarization function, that—in the static limit—is

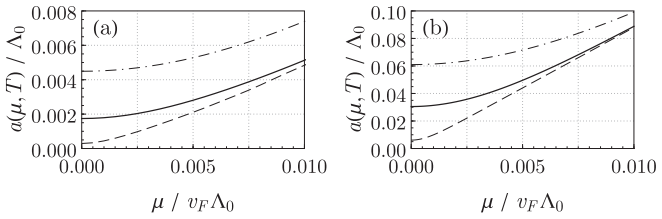

FIG. 3. Quantitative comparison between the (a) fully self-consistent solution and (b) one loop approximation of the coefficient function $a(\mu,T)$ for the reduced temperatures $T/v_F\Lambda_0 = 5\times10^{-4}, 2.5\times10^{-3}, 5\times10^{-3}$ (bottom to top data sets). In the small momentum regime, $q \ll T/v_F, \mu/v_F$, the static dielectric function shows a $1/q$ divergence according to $\epsilon_\mu(q \ll T/v_F) = 1 + a(\mu,T)\Lambda_0/q$. Observe that the self-consistent solution is about an order of magnitude smaller than the one-loop prediction.

independent of momentum and a function of temperature and chemical potential only [18],

$$\epsilon_\mu^{\text{1-loop}}(q \ll T/v_F) = 1 + a(\mu,T)\frac{\Lambda_0}{q}, \tag{7}$$

with

$$a(\mu,T) = 8\alpha\frac{T}{v_F\Lambda_0}\ln\left(2\cosh\frac{\mu}{2T}\right). \tag{8}$$

Here, the coefficient function $a(\mu,T)$ is directly proportional to the static limit of the polarization function. At the charge neutrality point $a(\mu,T)$ scales linearly with temperature, whereas for $\mu \gg T$ it becomes independent of temperature, scaling linearly with the chemical potential. The former feature has been shown to remain valid in a nonperturbative fRG calculation [16], showing a strong renormalization of the slope. To verify whether the latter feature remains valid beyond perturbation theory, we solved the self-consistency Eqs. (4) and (5) for the two additional temperatures $T/v_F\Lambda_0 = 5\times10^{-4}, 5\times10^{-3}$ and extracted the coefficient functions $a(\mu,T)$; see Fig. 3. For large chemical potentials we observed a transition into a linear regime, which is consistent with the result obtained by perturbation theory. However, the precise slope could not be determined sufficiently accurately due to convergence issues of the numerical integration: at very small momenta and increasingly large chemical potentials the integrand of Eq. (5) becomes very strongly peaked, such that limited machine precision becomes problematic. Nevertheless, our results indicate that the scaling behavior predicted by perturbation theory is indeed correct, albeit with a strongly renormalized slope. A precise estimation of the slope would require a recalculation of the temperature dependence of the renormalized Fermi velocity and dielectric function at the charge neutrality point with a better resolution and accuracy than what was achieved previously in Ref. [16].

The numerical results for the chemical potential dependence of the renormalized Fermi velocity are shown in Fig. 4. At the initial chemical potential $\mu_0 = 0$ the infrared divergence of the renormalized Fermi velocity is regularized due to the temperature-induced screening of the renormalized Coulomb interaction [16], while in the large momentum regime, $k \gg T/v_F$, the renormalized Fermi velocity shows the logarithmic

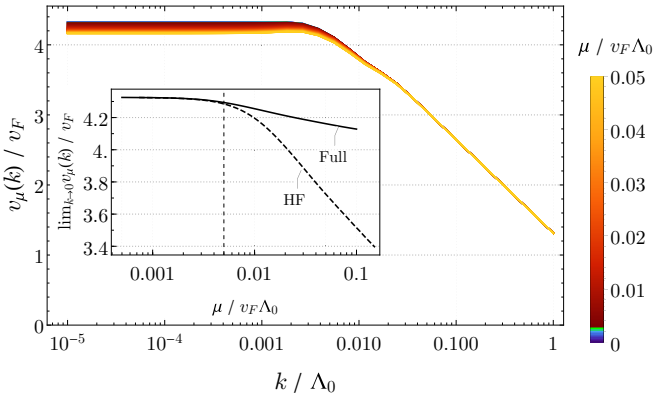

FIG. 4. Renormalized Fermi velocity $v_\mu(k)$ as a function of momentum and chemical potential at temperature $T/v_F\Lambda_0 = 2.5\times10^{-3}$ in the fully self-consistent calculation. The renormalized Fermi velocity is finite at $k = 0$ at the initial chemical potential $\mu_0 = 0$ due to temperature induced screening of the renormalized Coulomb interaction. Increasing the chemical potential away from the charge neutrality point shows a weak suppression of the Fermi velocity for small momenta. The inset shows a comparison between the $k \to 0$ limits of the Fermi velocity in the self-consistent treatment and in Hartree-Fock approximation as functions of the chemical potential. The dashed vertical line marks $\mu = 2T$. For $\mu > 2T$ both calculations show a logarithmic suppression of $v_\mu(k \to 0)$. This suppression is significantly weakened in the full computation when compared to the result of the Hartree-Fock approximation.

behavior [9,16]

$$v_{\mu=0}(k \gg T/v_F)/v_F = A + B\ln(\Lambda_0/k), \tag{9}$$

with $A = 1.34(4)$ and $B = 0.52(1)$. Upon increasing the chemical potential the solution shows a further, but only very weak suppression of the Fermi velocity at low momenta in accord with the assumption of Bauer *et al.* [9]. The other temperatures we investigated also show a negligible μ dependence (data not shown). Our full calculation allows us to understand this behavior by considering the combined effect of strong screening and the formation of a nontrivial Fermi surface. By increasing the chemical potential the additional charge carriers fill up the renormalized spectrum and introduce a circularly shaped Fermi surface, which is driven further and further away from the nodal point, while the renormalized Coulomb interaction becomes increasingly short ranged. As a result, the screened Coulomb interaction only operates near the Fermi surface and, loosely speaking, does not reach far enough down the spectrum to have a significant impact on the small momentum regime of the renormalized Fermi velocity. Neglecting the charge carrier-induced screening would cause a much stronger suppression of the Fermi velocity, since then the Coulomb interaction could reach down to the nodal point. In order to validate this picture we also performed a Hartree-Fock–like calculation of the velocity, see the inset of Fig. 4, where only Eq. (4) has been solved self-consistently for $\xi_\mu(k)$. The μ flow of the dielectric function therein was neglected and the function $\chi_\mu(q) = \epsilon_\mu(q)q$ was kept at its initial value $\chi_\mu(q) = \chi_{\mu_0=0}(q)$, where only temperature induced screening is present. The Hartee-Fock solution shows the same features as the fully self-consistent solution. However, the low momentum

regime of the Hartree-Fock Fermi velocity is much stronger suppressed, supporting the above reasoning. Our observations are also consistent with the findings from one-loop perturbation theory. As was shown in Ref. [17], at zero temperature a finite chemical potential regularizes the logarithmic divergence according to

$$v_\mu^{\text{1-loop}}(k=0)/v_F = 1 + \frac{\alpha}{4}\ln(\Lambda_0/k_F), \tag{10}$$

with the Fermi momentum $k_F = \mu/v_F$. Here, the suppression of the infrared divergence is much stronger than what we find in our self-consistent approach, since it is the bare, unscreened Coulomb interaction that enters their calculations. Although the intrinsic ($\mu = 0$) part of the self-energy leads to an infrared divergence as a function of momentum, it is immediately cut off by the extrinsic ($\mu \neq 0$) part of the self-energy, even for large μ, far away from the nodal point, due to the infinite range of the unscreened Coulomb interaction.

Since our data show that the Fermi velocity is virtually independent from the chemical potential in its entire momentum regime, the μ-flow fRG together with the truncation scheme used here is consistent with the approximation of Ref. [9]. However, the nigh μ independence of the velocity function we find is actually problematic and cannot hold for all values of the chemical potential, as the following line of arguments shows.

In the critical evaluation of our results for the chemical potential dependence of the Fermi velocity the main focus lies on the low momentum regime, in particular the zero momentum singularity found at zero temperature. In contrast to Ref. [17] we are working at finite temperature, which already provides a proper regularization of the logarithmic infrared divergence, making it necessary to distinguish the two regimes $\mu \ll T$ and $\mu \gg T$. In the regime $\mu \ll T$ the chemical potential should be irrelevant for the suppression of the logarithmic divergence, since there temperature induced screening dominates. Our numerical data fully support this intuition as can be seen in the inset of Fig. 4. This result may have already been anticipated from the analytical form of Eq. (4) prior to the numerical solution, since in this limit the inverse hyperbolic cosines in the integrand cancel each other, leading to a constant velocity as a function of the chemical potential. In the regime $\mu \gg T$, on the other hand, one should expect the suppression of the logarithmic divergence to be driven solely by the chemical potential—independent of temperature—in much the same way as the $1/q$ divergence of the dielectric function becomes temperature independent for large enough μ; cf. Fig. 3. It is unphysical that temperature controls the regularization of the infrared divergence far away from the charge neutrality point. Hence its influence should vanish in that regime. Although our data show a certain logarithmic suppression of $v_\mu(k=0)$ as a function of μ for all the temperatures investigated, the suppression itself is far too weak to be compatible with the expectation presented above.

As it stands our results show a certain "asymmetry" in how the small momentum regime of the Fermi velocity is affected by a finite temperature in comparison to a finite chemical potential, which contradicts physical intuition and should not be present. Based on the physics that is contained within our flow equations, as well as taking into account the arguments of the discussion at the end of the previous section, we, thus, conclude that the minimal truncation employed here is not capable of describing the proper chemical potential dependence of the Fermi velocity in the small momentum regime. Since both the chemical-potential flow theory and more standard fRG approaches are based on the same exact flow equation, whose approximative solutions converge to the same result in the exact theory, we are convinced that a higher order truncation of the chemical-potential flow equations will resolve these issues and lead to the expected behavior. To this end one should systematically improve our truncation by including the effects of the quasiparticle wave function renormalization and three-vertex renormalization (recall that those quantities are connected via a Ward identity), and possibly also the flow of the four-vertex. As an alternative to the Fermi-Bose framework employed here, one could also consider a purely fermionic formulation, which removes the bias introduced by the choice of a particular interaction channel via partial bosonization. In such a framework one would have to implement the initially nontrivial dielectric function as part of the initial fermionic four-vertex. Only if a truncation is able to produce a strong enough suppression of the small momentum components of the renormalized Fermi velocity, that becomes temperature independent upon increasing μ into the regime $\mu \gg T$, could it be claimed with confidence that the particularly chosen truncation is justified.

IV. CONCLUSIONS

The idea to use the chemical potential as a flow parameter in a functional renormalization group calculation was first put forward by Berges *et al.* [14] in the context of a particle-physics problem and since then has rarely been adopted by other authors; see, e.g., Ref. [15] for an application in condensed matter theory. We here have presented another application of the fRG with the chemical potential as the flow parameter in a condensed matter system. In contrast to the physical system investigated in Ref. [15] a separate nonperturbative calculation is required to establish the initial condition for the flow. This initial "investment" pays off, because for a chemical-potential based flow each point in the solution of the flow equation is of physical relevance, in contrast to more standard fRG approaches, where only the end point of the flow matters. The alternative would be to run a conventional fRG calculation for each value of the chemical potential separately. The two approaches should converge to the same result if the respective truncations are of sufficiently high order, but the standard fRG approach involves much greater effort to study a functional μ dependence. Nevertheless, it would be an important research topic to investigate this convergence issue systematically—be it for graphene or nonrelativistic Fermi liquids—by comparing the predictions of the two approaches for several truncations against each other. While the standard finite density fRG has already proven to be a reliable framework for a plethora of materials, the chemical-potential flow has—in our opinion—great potential, but lacks those numerous tests, which are necessary for this method to become a viable alternative.

We have applied the technique for the calculation of the carrier density dependence of the Fermi velocity and the static dielectric function in graphene, using a conventional fRG calculation at zero chemical potential as initial condition. Graphene is a very suitable context for an application of the

chemical-potential flow technique. In this material physical quantities in principle have a strong dependence of the carrier density, providing a need for such a calculation, while the high-symmetry point of zero carrier density brings significant simplifications, allowing for an efficient "conventional" non-perturbative calculation at that point. Our numerical results are consistent with the earlier work of Bauer *et al.* [9], which took the momentum-dependent Fermi velocity to be independent of the chemical potential for $n \lesssim k^2/\pi$, yielding practically identical fits to the experimental data of Elias *et al.* [8]. However, our approximations yield a suppression of the infrared divergence that is too weak to be compatible with the expected symmetry $\max(\mu, T)$, that is the divergence should be cut off by either the chemical potential or temperature, depending on which of these two quantities is larger, which we believe to be not physical. Although a stronger suppression of the small momentum regime should have little impact on the actual fit to the experimental data, most certainly not being able to invalidate it, further work is necessary to settle the issue satisfyingly. The dielectric function is, however, strongly dependent on the chemical potential, reflecting the strong carrier dependence of the screening length in graphene. For this observable we expect a higher order truncation to yield only minor modifications, since the main features that should occur at finite density—in particular the transition into a temperature independent regime for $\mu \gg T$—could already be observed. Even though the current truncation is not sufficient for the Fermi velocity, it appears to be a reasonable approximation to the static dielectric function. Once the issues for the Fermi velocity at small momenta are resolved, it would be interesting to apply our method to the three dimensional analog of graphene, the so-called Weyl semimetals. Such materials feature a conical spectrum as well and a chemical-potential based flow could be implemented equally efficiently.

ACKNOWLEDGMENTS

We thank Piet Brouwer and Björn Sbierski for support in the preparation of the manuscript. This work is supported by the German Research Foundation (DFG) in the framework of the Priority Program 1459 "Graphene."

APPENDIX A: DERIVATION OF THE CHEMICAL-POTENTIAL FLOW EQUATION

In this appendix, we explain some details about the general chemical potential flow theory, which is the basis for the flow equations (4) and (5). Since the theory relies on a reinterpretation of the chemical potential as a flow parameter, the main results can be transferred directly from Ref. [16].

The starting point for the derivation of an exact flow equation is the μ-dependent partition function $Z_\mu[\boldsymbol{\eta}, \boldsymbol{J}]$. It is defined as the functional Fourier transform of the exponentiated bare action $S_\mu[\boldsymbol{\psi}, \boldsymbol{\phi}]$ [13,20,22,32],

$$Z_\mu[\boldsymbol{\eta}, \boldsymbol{J}] = \int \mathcal{D}\boldsymbol{\psi}\mathcal{D}\boldsymbol{\psi}^\dagger\mathcal{D}\boldsymbol{\phi}\, e^{iS_\mu[\boldsymbol{\psi},\boldsymbol{\phi}]+i\boldsymbol{\eta}^\dagger\tau_1\boldsymbol{\Psi}+i\boldsymbol{\Psi}^\dagger\tau_1\boldsymbol{\eta}+i\boldsymbol{\phi}^\intercal\tau_1\boldsymbol{J}}. \tag{A1}$$

The bare action is a functional of fermionic and bosonic fields, which can be derived from the purely fermionic Hamiltonian (1) by a standard procedure [16,20–22]. The bosonic field is introduced by a Hubbard-Stratonovich transformation of the Coulomb interaction term in the density-density channel. The index μ indicates that both the partition function and the bare action depend on the chemical potential. The chemical potential dependence of the bare action enters explicitly via the quadratic μ term in the Hamiltonian and implicitly via the background density $\tilde{n}_\mu$. In contrast to the conventional fRG there is no additional infrared regulator [14]. Furthermore, we work in the real-time Keldysh formalism [25–32], which involves a doubling of degrees of freedom, with classical (c) and quantum (q) component for each field [16,21,22,32]

$$\boldsymbol{\Psi} \equiv \begin{pmatrix}\Psi_c & \Psi_q\end{pmatrix}^\intercal, \quad \boldsymbol{\Psi}^\dagger = (\boldsymbol{\Psi})^\dagger, \quad \boldsymbol{\phi} \equiv \begin{pmatrix}\phi_c & \phi_q\end{pmatrix}^\intercal. \tag{A2}$$

Lastly, $\boldsymbol{\eta}$ and $\boldsymbol{J}$ are fermionic and bosonic source fields, respectively. In Eq. (A1) we employed a condensed vector notation for the source terms, containing integration and summation of continuous and discrete field degrees of freedom implicitly, e.g.,

$$\boldsymbol{\eta}^\dagger\tau_1\boldsymbol{\Psi} \equiv \int_x \boldsymbol{\eta}^\dagger(x)\tau_1\boldsymbol{\Psi}(x), \tag{A3}$$

where τ_1 is a Pauli matrix acting in Keldysh space.

The effective action may now be introduced as the modified Legendre transform of the connected functional $W_\mu[\boldsymbol{\eta}, \boldsymbol{J}] = -i \ln Z_\mu[\boldsymbol{\eta}, \boldsymbol{J}]$ [10–14],

$$\begin{aligned}\Gamma_\mu[\boldsymbol{\psi},\boldsymbol{\phi}] = W_\mu[\boldsymbol{\eta}_\mu, \boldsymbol{J}_\mu] - \boldsymbol{\eta}_\mu^\dagger\tau_1\boldsymbol{\Psi} - \boldsymbol{\Psi}^\dagger\tau_1\boldsymbol{\eta}_\mu - \boldsymbol{\phi}^\intercal\tau_1\boldsymbol{J}_\mu \\ - \boldsymbol{\Psi}^\dagger\hat{\boldsymbol{R}}_\mu\boldsymbol{\Psi},\end{aligned} \tag{A4}$$

with

$$\hat{\boldsymbol{R}}_\mu(x,y) = \begin{pmatrix}0 & \mu\,\delta(x-y)\hat{\mathbb{1}} \\ \mu\,\delta(x-y)\hat{\mathbb{1}} & 0\end{pmatrix}. \tag{A5}$$

The term $\boldsymbol{\Psi}^\dagger\hat{\boldsymbol{R}}_\mu\boldsymbol{\Psi}$ is the explicit chemical-potential term one obtains in the bare action $S_\mu[\boldsymbol{\psi},\boldsymbol{\phi}]$. Its resemblance with an additive infrared regulator in the conventional fRG is the foundation of the chemical-potential flow theory [14,15]. According to the usual definition of the effective flowing action, the "chemical-potential regulator term" has been subtracted on the right hand side [10–14]. Consequently, the effective action Γ_μ involves flowing vertex functions only, and the explicit chemical-potential term—in comparison to the bare action—is absent. Note that some authors prefer to include a finite chemical potential in the fermionic distribution function, rather than in the spectral part of the inverse propagators as we do here [22]. Such an alternative choice would affect the structure of the regulator (A5) and the vertex expansion of the effective action, but it cannot lead to any observable consequences, since these two choices are connected by a (time dependent) gauge transformation.

The exact chemical-potential flow equation follows immediately upon taking the μ derivative of Eq. (A4), keeping the

fields $\boldsymbol{\psi}$ and $\boldsymbol{\phi}$ fixed,

$$\partial_\mu \Gamma_\mu[\boldsymbol{\psi},\boldsymbol{\phi}] = \frac{i}{2}\partial\!\!\!/_\mu \mathrm{STr}\ln\big(\hat{\boldsymbol{\Gamma}}^{(2)}_\mu[\boldsymbol{\psi},\boldsymbol{\phi}] + \hat{\boldsymbol{\mathcal{R}}}_\mu\big) + 2\phi_q \partial_\mu \tilde{n}_\mu, \tag{A6}$$

where $\hat{\boldsymbol{\Gamma}}^{(2)}_\mu$ is a Hesse matrix of second derivatives, and

$$\hat{\boldsymbol{\mathcal{R}}}_\mu \equiv \mathrm{diag}\big(-\hat{\boldsymbol{R}}_\mu, \hat{\boldsymbol{R}}^{\mathsf{T}}_\mu, 0\big). \tag{A7}$$

The "single-scale derivative" $\partial\!\!\!/_\mu$ in Eq. (A6) only acts on the regulator $\hat{\boldsymbol{\mathcal{R}}}_\mu$. The above flow equation is the Keldysh analog of the original, imaginary-time flow equation proposed by Berges *et al.* [14]. We note here that the initial condition for this exact flow equation is given by the exact effective action (A4) at some arbitrarily chosen initial chemical potential μ_0. As already stressed in the main text, this initial condition has to be calculated separately by other nonperturbative techniques, since the "chemical potential regulator" does not provide an infrared regularization in the standard fRG sense.

APPENDIX B: VERTEX FLOW EQUATIONS AND ONE-LOOP APPROXIMATION

The flow equations for the one-particle irreducible vertex functions are obtained by expanding the effective action in powers of fields, which needs to be inserted into the above equation, and comparing coefficients [12,13,16]. Since we are only interested in thermal equilibrium, where the fluctuation-dissipation theorem holds [22], we only need to consider the resulting flow equations for the retarded components of the self-energy and polarization function. In a condensed notation, where numerical arguments denote space and time coordinates, $1 \equiv (\vec{r}_1, t_1)$, and latin indices encompass the discrete fermionic degrees of freedom, sublattice, valley, and spin, these flow equations read

$$\partial_\mu \Sigma^R_{\mu,ij}(1,2) = i\partial\!\!\!/_\mu \sum_{k,l} \int' \big(\Gamma^{qcc}_{\mu,ik}(1,1';4') G^K_{\mu,kl}(1',2') \Gamma^{ccq}_{\mu,lj}(2',2;3') D^A_\mu(3',4') + \Gamma^{qcc}_{\mu,ik}(1,1';4') G^R_{\mu,kl}(1',2') \Gamma^{qcc}_{\mu,lj}(2',2;3') D^K_\mu(3',4')\big), \tag{B1}$$

$$\partial_\mu \Pi^R_\mu(1,2) = \frac{i}{2}\partial\!\!\!/_\mu \sum_{k,l,m,n} \int' \big(G^K_{\mu,kl}(1',2') \Gamma^{ccq}_{\mu,lm}(2',3';1) G^R_{\mu,mn}(3',4') \Gamma^{qcc}_{\mu,nk}(4',1';2) + G^A_{\mu,kl}(1',2') \Gamma^{ccq}_{\mu,lm}(2',3';1) G^K_{\mu,mn}(3',4') \Gamma^{cqc}_{\mu,nk}(4',1';2)\big). \tag{B2}$$

The functions $\Gamma^{\alpha\beta\gamma}_{\mu,ij}(1,2;3)$, with $\alpha,\beta,\gamma = c,q$, are the Fermi-Bose three-vertices of the theory in the real-time Keldysh formulation. The primed integration sign indicates that all primed arguments have to be integrated. Here, the contributions to the flow from four-vertices has already been neglected. A transformation to Fourier space is beneficial, due to energy and momentum conservation. The flowing frequency-momentum space propagators that enter the transformed flow equations read

$$\hat{G}^{R/A}_\mu(\vec{k},\varepsilon) = \frac{1}{\sigma^s_0 \otimes \big(\varepsilon + \mu - v_F \vec{\Sigma}\cdot\vec{k} - \hat{\Sigma}^{R/A}_\mu(\vec{k},\varepsilon)\big)}, \tag{B3a}$$

$$\hat{G}^K_\mu(\vec{k},\varepsilon) = \tanh\frac{\varepsilon}{2T}\big(\hat{G}^R_\mu(\vec{k},\varepsilon) - \hat{G}^A_\mu(\vec{k},\varepsilon)\big), \tag{B3b}$$

$$D^{R/A}_\mu(\vec{q},\omega) = \frac{1}{2}\frac{1}{V^{-1}(\vec{q}) + \Pi^{R/A}_\mu(\vec{q},\omega)}, \tag{B4a}$$

$$D^K_\mu(\vec{q},\omega) = \coth\frac{\omega}{2T}\big(D^R_\mu(\vec{q},\omega) - D^A_\mu(\vec{q},\omega)\big). \tag{B4b}$$

The single-scale derivative in Eqs. (B1) and (B2) only acts on the flowing fermionic propagators, substituting the latter by a single-scale propagator

$$\partial\!\!\!/_\mu \hat{G}^{R/A}_\mu(\vec{k},\varepsilon) = -\big(\hat{G}^{R/A}_\mu(\vec{k},\varepsilon)\big)^2. \tag{B5}$$

Here, the μ dependence of the flowing self-energy is held constant upon taking the single-scale derivative $\partial\!\!\!/_\mu$. By using the approximations mentioned in the main text—that is, setting all the three-vertices to unity as well as neglecting any dynamical effects—and employing all the symmetries, after a straightforward calculation we arrive at the flow equations (4) and (5).

As an important crosscheck of the formalism, it is desirable to reproduce the results of the one-loop approximation of diagrammatic perturbation theory directly within the chemical-potential flow framework. To this end one should neglect the chemical potential dependence of the three-vertices, setting them to their (noninteracting) initial value at $\mu = 0$, and one should replace the interacting flowing propagators in the flow equations (B1) and (B2) by their noninteracting counterparts, Eqs. (B3a)–(B4b) with $\hat{\Sigma}^{R/A}_\mu$ and $\Pi^{R/A}_\mu$ set to zero. It is then possible to perform the summations and integrations on the right hand side of the flow equations analytically exactly, such that—in real-space representation—one is left with simple algebraic products of noninteracting propagators. Furthermore, with these approximations the single-scale derivative $\partial\!\!\!/_\mu$ turns into an ordinary partial derivative ∂_μ, since the remaining terms do not contain any nontrivial μ dependences apart from the one given by the chemical potential regulator within the noninteracting flowing propagators. Thus the above flow equations reduce to the simple form

$$\partial_\mu \hat{\Sigma}^R_\mu(1,2) = i\,\partial_\mu\big(\hat{G}^R_{0,\mu}(1,2) D^K_{0,\mu}(2,1) + \hat{G}^K_{0,\mu}(1,2) D^A_{0,\mu}(2,1)\big), \tag{B6}$$

$$\partial_\mu \Pi^R_\mu(1,2) = \frac{i}{2}\partial_\mu \mathrm{tr}\big(\hat{G}^R_{0,\mu}(1,2)\hat{G}^K_{0,\mu}(2,1) + \hat{G}^K_{0,\mu}(1,2)\hat{G}^A_{0,\mu}(2,1)\big), \tag{B7}$$

which is nothing but a differential form of the well-known one-loop result for the fermionic self-energy and bosonic polarization function [22]. Here, the subscript "0" at the propagators indicates that they are the noninteracting ones, and the trace in Eq. (B7) covers the discrete fermionic degrees of freedom: sublattice, valley, and spin. The one-loop flow equations may be integrated trivially to obtain the results of diagrammatic perturbation theory. To be consistent with the one-loop approximation one should employ the perturbative results for the initial condition at $\mu = 0$ on the left hand side of the integrated flow equations: $\hat{\Sigma}^R_{\mu=0} = (\hat{\Sigma}^R_{\mu=0})_{1\text{-loop}}$ and $\Pi^R_{\mu=0} = (\Pi^R_{\mu=0})_{1\text{-loop}}$. The above one-loop self-energy has been obtained in Ref. [17], albeit in the imaginary time Matsubara formalism at zero temperature, showing that the logarithmic zero momentum divergence found at charge neutrality is regularized by a finite chemical potential; cf. Eq. (10). The one-loop polarization function at finite temperature and density has been calculated in Ref. [18] also within the Keldysh formalism.

[1] P. R. Wallace, Phys. Rev. **71**, 622 (1947).
[2] G. W. Semenoff, Phys. Rev. Lett. **53**, 2449 (1984).
[3] A. H. Castro Neto, F. Guinea, N. M. R. Peres, K. S. Novoselov, and A. K. Geim, Rev. Mod. Phys. **81**, 109 (2009).
[4] J. González, F. Guinea, and M. A. H. Vozmediano, Nucl. Phys. B **424**, 595 (1994).
[5] J. González, F. Guinea, and M. A. H. Vozmediano, Phys. Rev. B **59**, R2474(R) (1999).
[6] M. A. H. Vozmediano, Philos. Trans. R. Soc. London A **369**, 2625 (2011).
[7] V. N. Kotov, B. Uchoa, V. M. Pereira, F. Guinea, and A. H. Castro Neto, Rev. Mod. Phys. **84**, 1067 (2012).
[8] D. C. Elias, R. V. Gorbachev, A. S. Mayorov, S. V. Morozov, A. A. Zhukov, P. Blake, L. A. Ponomarenko, I. V. Grigorieva, K. S. Novoselov, F. Guinea, and A. K. Geim, Nat. Phys. **7**, 701 (2011).
[9] C. Bauer, A. Rückriegel, A. Sharma, and P. Kopietz, Phys. Rev. B **92**, 121409(R) (2015).
[10] C. Wetterich, Int. J. Mod. Phys. A **16**, 1951 (2001).
[11] J. Berges, N. Tetradis, and C. Wetterich, Phys. Rep. **363**, 223 (2002).
[12] W. Metzner, M. Salmhofer, C. Honerkamp, V. Meden, and K. Schönhammer, Rev. Mod. Phys. **84**, 299 (2012).
[13] P. Kopietz, L. Bartosch, and F. Schütz, *Introduction to the Functional Renormalization Group* (Springer, New York, 2010).
[14] J. Berges, D.-U. Jungnickel, and C. Wetterich, Int. J. Mod. Phys. A **18**, 3189 (2003).
[15] F. Sauli and P. Kopietz, Phys. Rev. B **74**, 193106 (2006).
[16] C. Fräßdorf and J. E. M. Mosig, Phys. Rev. B **95**, 125412 (2017).
[17] E. H. Hwang, B. Y.-K. Hu, and S. Das Sarma, Phys. Rev. Lett. **99**, 226801 (2007).
[18] M. Schütt, P. M. Ostrovsky, I. V. Gornyi, and A. D. Mirlin, Phys. Rev. B **83**, 155441 (2011).
[19] V. P. Gusynin, S. G. Sharapov, and J. P. Carbotte, Int. J. Mod. Phys. B **21**, 4611 (2007).
[20] J. W. Negele and H. Orland, *Quantum Many-Particle Systems* (Westview Press, Boulder, CO, 1998).
[21] G. Schwiete and A. M. Finkel'stein, Phys. Rev. B **89**, 075437 (2014).
[22] A. Kamenev, *Field Theory of Non-Equilibrium Systems* (Cambridge University Press, Cambridge, UK, 2011).
[23] C. Popovici, C. S. Fischer, and L. von Smekal, Phys. Rev. B **88**, 205429 (2013).
[24] There are cases, however, where a certain initial reference point can lead to significant simplifications. For example, in the study of the low density regime of the two-dimensional electron gas performed in Ref. [15], the initial chemical potential $\mu_0 = 0$ corresponds to the case of vanishing particle density, implying that the self-energy vanishes identically and the effective interaction is obtained via a resummation of particle-particle ladder diagrams.
[25] R. Gezzi, T. Pruschke, and V. Meden, Phys. Rev. B **75**, 045324 (2007).
[26] S. G. Jakobs, V. Meden, and H. Schoeller, Phys. Rev. Lett. **99**, 150603 (2007).
[27] T. Gasenzer and J. M. Pawlowski, Phys. Lett. B **670**, 135 (2008).
[28] J. Berges and G. Hoffmeister, Nucl. Phys. B **813**, 383 (2009).
[29] C. Karrasch, M. Pletyukhov, L. Borda, and V. Meden, Phys. Rev. B **81**, 125122 (2010).
[30] T. Kloss and P. Kopietz, Phys. Rev. B **83**, 205118 (2011).
[31] D. M. Kennes, S. G. Jakobs, C. Karrasch, and V. Meden, Phys. Rev. B **85**, 085113 (2012).
[32] J. Berges and D. Mesterházy, Nucl. Phys. B Proc. Suppl. **228**, 37 (2012).
[33] Although for $\mu_0 = 0$ the renormalization of the Fermi surface is trivial, the spectrum around charge neutrality is still renormalized nontrivially, which yields a significant contribution to the renormalization of the Fermi surface at μ found after flowing from $\mu_0 = 0$ to μ. If one would want to initialize the flow at some finite μ_0 instead, then the calculation of the initial condition has to incorporate a—now nontrivial—renormalization towards the interacting Fermi surface at μ_0.
[34] Depending on the sign of μ, the interacting Fermi surface, being a circle of radius k_F, is located either within the conduction or valence band.
[35] Within the standard finite-density fRG approach one typically employs a purely fermionic formulation, taking into account the flow of the full four-vertex, in combination with so-called patching techniques. Such a formulation has the advantage that it does not favor a particular interaction channel, in contrast to a theory containing a Hubbard-Stratonovich boson. Although the Hubbard-Stratonovich transformation is an exact integral identity, it introduces a certain bias towards a particular interaction channel once the hierarchy of flow equations is truncated (especially if truncated at a low level).